









Article

Observational Evidence of Intensified Extreme Seasonal Climate Events in a Conurbation Area Within the Eastern Amazon

Everaldo Barreiros de Souza ^{1,2,*} , Douglas Batista da Silva Ferreira ³ , Ana Paula Paes dos Santos ³ , Alan Cavalcanti da Cunha ⁴ , João de Athaydes Silva Junior ¹, Alexandre Melo Casseb do Carmo ¹ , Victor Hugo da Motta Paca ⁵ , Thaiane Soeiro da Silva Dias ² , Waleria Pereira Monteiro Correa ² and Tercio Ambrizzi ⁶ 

- ¹ Faculdade de Meteorologia, Instituto de Geociências, Universidade Federal do Pará, Belém 66075-110, PA, Brazil; athaydes@ufpa.br (J.d.A.S.J.); casseb@ufpa.br (A.M.C.d.C.)
 - ² Programa de Pós-Graduação em Ciências Ambientais, Instituto de Geociências, Universidade Federal do Pará, Belém 66075-110, PA, Brazil; thaiane.dias24@gmail.com (T.S.d.S.D.); waleriapmonteiro@gmail.com (W.P.M.C.)
 - ³ Instituto Tecnológico Vale, Belém 66055-090, PA, Brazil; douglas.silva.ferreira@itv.org (D.B.d.S.F.); ana.santos@pq.itv.org (A.P.P.d.S.)
 - ⁴ Departamento de Engenharia Civil, Universidade Federal do Amapá, Macapá 68900-070, AP, Brazil; alancunha@unifap.br
 - ⁵ Serviço Geológico do Brasil, Rio de Janeiro 22290-240, RJ, Brazil; victorpaca@yahoo.com
 - ⁶ Instituto de Astronomia, Geofísica e Ciências Atmosféricas, Universidade de São Paulo, São Paulo 05508-010, SP, Brazil; tercio.ambrizzi@iag.usp.br
- * Correspondence: everaldo@ufpa.br

Abstract

This study presents an integrated assessment of four decades (1985–2023) of environmental and climate alterations in the principal metropolitan conurbation of the eastern Brazilian Amazon, encompassing Belém and its adjacent municipalities. By combining high-resolution land use/land cover (LULC) dynamics with in situ meteorological data, including understudied elements, such as relative humidity (RH) and wind speed, and satellite-derived precipitation estimates (CHIRPS v3), we advance the scientific understanding of regional climate trends. Our results document significant climate shifts, including pronounced dry-season warming (+1.5 °C), atmospheric drying (−4% in RH), attenuated wind patterns (−0.4 m s^{−1}), and altered precipitation regimes, which exhibit strong spatiotemporal coupling with extensive forest loss (−20%) and rapid urban expansion (+84%) between 1985 and 2023. Multivariate analyses reveal that these land–climate interactions are strongest during the dry regime, underscoring the role of surface–atmosphere feedbacks in amplifying regional changes. Comparative analysis of past (1980–1999) and present (2005–2024) decades demonstrates a marked intensification in the frequency and magnitude of extreme seasonal climate events. These findings elucidate a critical feedback mechanism that exacerbates climate risks in tropical urban areas. Consequently, we argue that mitigation public policies must prioritize the strict conservation of peri-urban forest fragments (vital for moisture recycling and local climate regulation) and the strategic implementation of green infrastructure aligned with prevailing wind patterns to enhance thermal comfort and resilience to hydrological extremes.

Keywords: urban climate; land-use change; Amazon; climate extremes; CHIRPS3



Academic Editor: Ashraf Dewan

Received: 26 August 2025

Revised: 20 September 2025

Accepted: 23 September 2025

Published: 25 September 2025

Citation: de Souza, E.B.; Ferreira, D.B.d.S.; Santos, A.P.P.d.; Cunha, A.C.d.; Silva Junior, J.d.A.; do Carmo, A.M.C.; Paca, V.H.d.M.; Dias, T.S.d.S.; Correa, W.P.M.; Ambrizzi, T.

Observational Evidence of Intensified Extreme Seasonal Climate Events in a Conurbation Area Within the Eastern Amazon. *Earth* **2025**, *6*, 112. <https://doi.org/10.3390/earth6040112>

Copyright: © 2025 by the authors.

Licensee MDPI, Basel, Switzerland.

This article is an open access article

distributed under the terms and

conditions of the Creative Commons

Attribution (CC BY) license

(<https://creativecommons.org/licenses/by/4.0/>).

1. Introduction

The anthropogenic transformation of land use and land cover (LULC) has emerged as a dominant driver of climate variations across global tropical regions, with consequent deforestation leading to measurable increases in near-surface air temperature and alterations of precipitation regimes [1]. In the Brazilian Amazon, unprecedented environmental changes coincide with an increasing frequency of extreme climate events, whose origins are linked to complex interactions involving global climate change, natural climate variability patterns, and regional-scale land surface modifications that have triggered multiple deforestation processes throughout the biome [2–4]. A recent study documented significant hydroclimate impacts in the Amazon, including intensification of both drought and flood episodes, accompanied by persistent warming trends [5].

While existing research has predominantly examined climate–environment interactions at the biome or basin scales, growing evidence suggests that urbanizing regions may experience amplified climate impacts through unique land–atmosphere feedback mechanisms. The eastern Amazon presents a critical but understudied scenario where rapid and intense urbanization intersects with intact or fragmented forest ecosystems [6], creating heterogeneous landscape mosaics that may generate novel environmental/climate dynamics, a research gap recently emphasized by the Science Panel for the Amazon [7]. Nevertheless, the current understanding on the urban climate in large Amazonian cities, such as Manaus and Belém, remains constrained by a predominant focus on near-surface temperature and precipitation extremes [8–11], despite evidence from tropical climatology on the fundamental role of atmospheric humidity and surface wind patterns in governing boundary-layer stability and modulating local circulations and convective processes [12]. This restricted observational scope is particularly critical in moist tropical cities, where humidity–wind interactions can directly influence thermal comfort and the potential for extreme climate in urbanized areas. Therefore, to address these multivariate knowledge gaps, with the intention of providing a more robust and mechanistic understanding of Amazonian urban climate, this work presents a comprehensive analysis of four decades of LULC changes combined with in situ and satellite-derived meteorological data across the most densely urbanized region of the eastern Brazilian Amazon. Our integrated approach advances current scientific understanding by (1) characterizing long-term changes in seasonal climatological regimes; (2) quantifying spatiotemporal patterns of LULC changes, with particular emphasis on demonstrating the conurbation process in the neighboring cities of Belém; (3) evaluating multivariate interactions between environmental and climate variables beyond air temperature and precipitation, including relative humidity and wind speed; and (4) assessing shifts in the magnitude and frequency of extreme seasonal climate events. The research focuses on the Belém conurbation, recognized as the oldest and most densely populated urban agglomeration in the Amazon estuary. This area exhibits a distinct historical pattern of urbanization occurring within a complex mosaic of primary/secondary forest and extensive water bodies, creating a spatial gradient of land-use change that is ideal for studying land–atmosphere interactions of global scientific relevance. By synthesizing these analytical dimensions, this work provides novel insights into contemporary urban climatology while establishing a methodological framework for assessing hazard risks, with immediate implications for designing mitigation strategies and climate-adaptive planning in the vulnerable and rapidly urbanizing forest-frontier cities.

2. Materials and Methods

2.1. Study Area and Observational Data

Figure 1 presents a map of the study area, encompassing the municipalities of Belém (BE), the state capital, Ananindeua (AN), Marituba (MA), and Benevides (BN), situated in

northeastern Pará state within the eastern Brazilian Amazon. The region is characterized by an extensive hydrographic network, with Guajará Bay and the Guamá River bordering the eastern margin of BE and the southern sectors of AN, MA, and BN, where elevations remain below 10 m. The principal terrestrial connectivity between Belém and adjacent municipalities is facilitated by the federal highway, which traverses the region diagonally, linking urban centers (municipal seats) situated on topographically elevated terrain (15–20 m). The 3D visualization highlights the expansive conurbation spanning from BE to BN, covering a linear extent of approximately 30 km. According to the 2022 IBGE Census, the combined population of the four municipalities totaled ~1.96 million inhabitants; however, recent official estimates for 2024 indicate growth to 2.1 million [13].

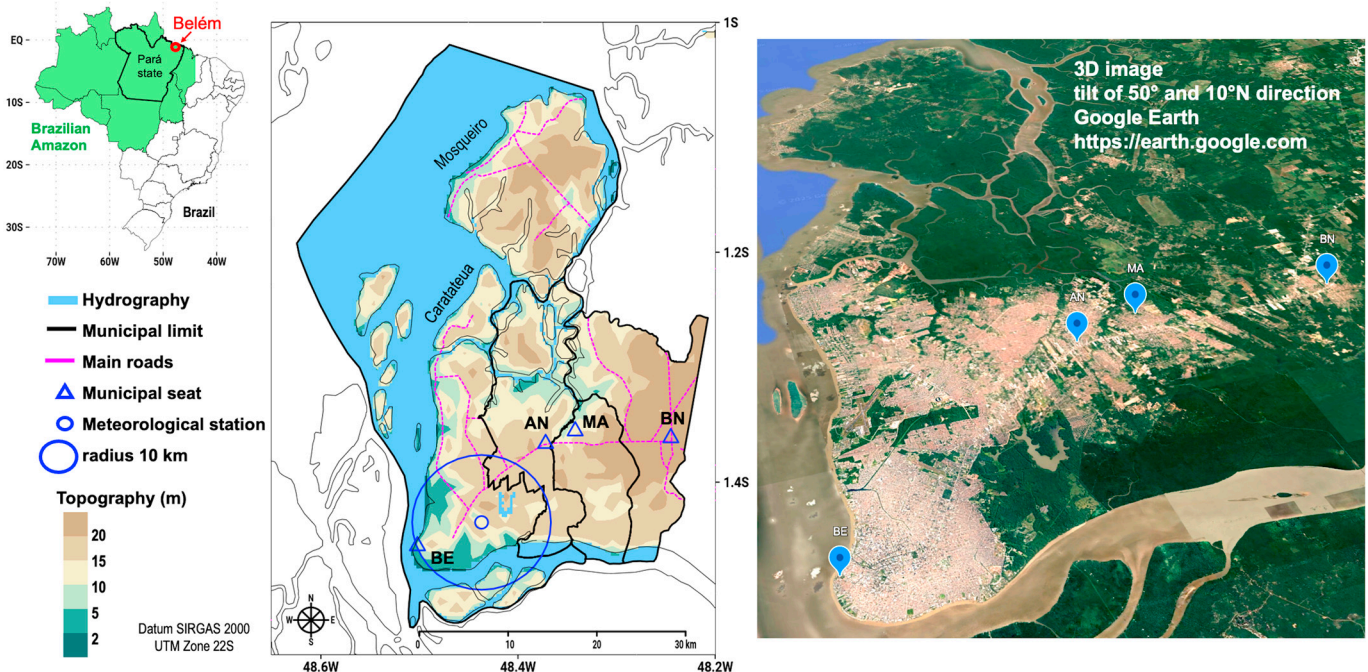


Figure 1. Study area encompassing the municipalities BE, AN, MA, and BN, with topography, hydrography, the main roads, and the locations of municipal seats and the INMET meteorological station (including a 10 km radius). Caratateua and Mosqueiro, larger islands north of BE, are indicated on the map. The 3D image illustrates the conurbation area connecting the four municipalities (Source: Google Earth <https://earth.google.com>, accessed on 1 July 2025).

Within the study area, only one conventional surface meteorological station, operated by the Instituto Nacional de Meteorologia (INMET; <https://bdmep.inmet.gov.br>, accessed on 6 January 2025), provides continuous, high-quality historical records of essential atmospheric variables (see Figure 1 for location). We utilized INMET station data spanning from January 1980 to December 2024, comprising in situ measurements of precipitation (P , mm), maximum (T_X , °C) and minimum (T_N , °C) air temperature, relative humidity (RH , %), and wind speed (WS , $m\ s^{-1}$), thus enabling climatological analysis over a 45-year period. According to World Meteorological Organization (WMO) standards, the rain gauge measuring P is located at a height of 1.5 m; the thermometers and the psychrometer measuring T_X , T_N , and RH are located inside the meteorological shelter at a height of 1.2 m; and the anemometer measuring WS is located in a mini tower at a height of 10 m above the ground. The reliance on a single in situ station is a common constraint in Amazonian climate studies due to the region's notoriously sparse observational network [14]. Although only one station is available, its 45-year continuous series provides unparalleled temporal

consistency, and the station's 10 km radius of representativeness (Figure 1) adequately captures the core urban climate signal of the conurbation in the region.

To complement observational analysis, we incorporated the Climate Hazards Group InfraRed Precipitation with Station (CHIRPS) dataset, a state-of-the-art quasi-global precipitation product that integrates satellite remote sensing with in situ station data to generate high-resolution (0.05°) estimates [15]. Validated extensively across tropical regions, CHIRPS demonstrates exceptional utility in data-sparse environments such as the Amazon [14,16], reliably capturing both synoptic-scale patterns and localized convective regimes. This makes it particularly suitable for climate trend analysis and hydrological studies in complex tropical ecosystems. Notably, this study employs the latest CHIRPS v3.0 (2024 release; <https://data.chc.ucsb.edu/products/CHIRPS/v3.0/>, accessed on 27 January 2025), marking the first application of this version in Amazonian precipitation studies. The refined CHIRPS3 algorithm exhibits improved performance in estimating a broader dynamic range of precipitation intensities.

Land use and land cover (LULC) data were derived from MapBiomas Collection 9 (<https://plataforma.brasil.mapbiomas.org>, accessed on 20 February 2025), which provides annual 30 m resolution classifications for Brazil through advanced machine learning algorithms applied to Landsat-5/7/8/9 and Sentinel-2 imagery [17]. Data processing was conducted via Google Earth Engine, utilizing the MapBiomas User Toolkit (<https://github.com/mapbiomas-brazil/user-toolkit>, accessed on 24 February 2025) with a standardized workflow: (i) spatial subsetting of imagery using municipal boundaries (BE, AN, MA, BN) via georeferenced shapefiles; (ii) application of the MapBiomas classification schema through remapping; and (iii) generation of annual composites (1985 to 2023) using quality mosaics. Our analysis focused on five critical LULC classes: (1) Forest formation (primary and secondary vegetation); (2) Pasture or farming (areas dedicated to growing crops and raising livestock); (3) Grassland or wetland (non-forest natural formations); (4) Urban infrastructure (built-up and impervious surfaces); and (5) Water bodies. Recent works have validated the data provided by MapBiomas with other independent environmental satellite data, particularly for the Belém metropolitan area, with consistent mapping results in the region [6,10,11].

2.2. Climatological Means and Definitions of Seasonal Regimes

The monthly means for all meteorological variables at the Belém station were calculated for the 30-year climatological normal (1991 to 2020), as recommended by the World Meteorological Organization [18]. The annual mean (all months) for P was also computed, and this threshold was used to distinguish seasonal regimes: the Wet regime includes consecutive months with P above the annual mean, and the Dry regime includes the remaining months with P below the annual mean. Climatological maps of P CHIRPS3 were generated for analysis of the spatial pluviometric distribution during the Wet and Dry regimes.

2.3. Correlation and Principal Component Analysis

Correlation analysis was used to quantify the relationships between environmental data (LULC classes) and key climate variables in the Belém region (P, TX, TN, RH, and WS), as a way to understand how territorial transformations impact local climate patterns in the Amazon region [19]. The Pearson correlation coefficient (r) measures linear association strength:

$$r_{xy} = \frac{\sum((x_i - x_m)(y_i - y_m))}{\sqrt{(\sum(x_i - x_m)^2) \sum(y_i - y_m)^2}} \quad (1)$$

where x_i and y_i are the individual monthly observations with pairs of environmental and climate variables, and x_m and y_m are climatological means.

The annual LULC data (Forest, Pasture, and Urban areas) and the seasonal climate data for P, TX, TN, RH, and WS in the Wet and Dry regimes were subjected to correlation calculations for the years 1985 to 2023 (a period of temporal coincidence of all variables). The statistical significance of correlation coefficients was tested using the t-statistic, following a distribution with $(n - 2)$ degrees of freedom. In addition to tables presenting quantitative results that emphasize statistically significant correlations, correlograms were constructed with numerical correlation values overlaid on color-coded cells for precise interpretation of all pairs of variables studied.

Complementing the investigation of multivariate relationships between environmental and climate variables in the Belém region, we implemented Principal Component Analysis (PCA), a multivariate statistical technique that transforms a set of potentially correlated variables into a smaller number of uncorrelated components that capture the maximum variance in the original dataset [20]. The application of this technique to LULC–climate interactions is particularly relevant in tropical regions like the Amazon, where strong land–atmosphere coupling allows deforestation and urbanization processes to modify precipitation regimes and air temperature patterns [21]. The analysis incorporated three LULC categories (annual Forest, Pasture, and Urban areas) and five climate variables (seasonal P, TX, TN, RH, and WS for Wet and Dry regimes) in the period from 1985 to 2023. Prior to PCA application, all variables were standardized using the Z-score transformation to ensure equal weighting across variables with different units and scales:

$$Z_{ij} = (x_{ij} - x_{mj})/s_j \quad (2)$$

where Z_{ij} is the standardized value for observation i and variable j , x_{ij} is the original observation, x_{mj} is the arithmetic mean of variable j , and s_j represents the standard deviation.

PCA was performed on the correlation matrix R as follows:

$$R = (1/(n - 1)) Z^T Z \quad (3)$$

where Z is the standardized data matrix, n is the number of observations, and Z^T denotes the transpose of Z .

The determinant of the correlation matrix serves as an indicator of multicollinearity among variables, with values approaching zero indicating substantial intercorrelation favorable for PCA application. Low determinant values confirm the presence of substantial intercorrelation among variables, validating the appropriateness of PCA for dimensionality reduction in the dataset. The principal components were extracted as the eigenvectors of the correlation matrix, with corresponding eigenvalues representing the variance explained by each component:

$$R v_k = \lambda_k v_k \quad (4)$$

where v_k is the eigenvector (principal component, PC), λ_k represents the eigenvalue, and k is the number of variables.

Eigenvalues quantify the variance explained by each principal component, while eigenvectors define the linear combinations of original variables constituting each component. The principal components are ordered by decreasing eigenvalue magnitude, ensuring that PC1 explains the maximum variance, PC2 explains the maximum remaining variance orthogonal to PC1, and so on. To determine the optimal number of principal components for retention, we used the Kaiser Criterion ($\lambda > 1.0$): components with eigenvalues exceeding unity were retained, yielding two significant components for both seasonal datasets. Additionally, the first two principal components explained over 70% of the variance, meeting

the Cumulative Variance Threshold [20]. The component loadings represent the correlation between original variables and principal components:

$$\text{Loading}_{jk} = \text{corr}(X_j, \text{PC}_k) \quad (5)$$

where X_j is the original variable j , and PC_k is the principal component k .

2.4. Mann–Kendall Test

For long-term trend analyses, we applied the Mann–Kendall test, a non-parametric statistical approach for detecting monotonic trends in time series data, particularly advantageous for climatological applications due to its independence from distributional assumptions and resilience to outliers [22]. The test statistic S (Equation (6)) quantifies the cumulative concordance between all possible pairs of observations, where the sign function $\text{sgn}(\theta)$ equals +1, 0, or −1 for positive, zero, or negative differences, respectively. Under the null hypothesis of no trend, the variance of S (Equation (7)) accounts for tied observations, where g represents the number of tied groups and t_i denotes the number of observations within each group.

$$S = \sum_{i=1}^{n-1} \sum_{j=i+1}^n \text{sgn}(x_j - x_i) \quad (6)$$

$$\text{Var}(S) = [n(n-1)(2n+5) - \sum_{i=1}^g t_i(t_i-1)(2t_i+5)]/18 \quad (7)$$

The standardized test statistic Z follows a standard normal distribution for large samples ($n \geq 10$), enabling hypothesis testing at predetermined significance levels. Sen's slope estimator [23] was employed for quantifying the trend magnitude by computing the median of all pairwise slopes $Q_k = (x_j - x_i)/(j - i)$ for $i < j$, yielding $N = n(n-1)/2$ slope estimates.

2.5. Comparisons Between Past and Current Decades and Analysis of Extreme Events

By comparing the descriptive statistics between the past and the recent decades (2010s and 2020s), the changes and temporal shifts in all meteorological variables were quantified and statistically evaluated in the Belém region, with particular emphasis on seasonal differences between the Wet (December–May) and Dry (June–November) regimes. The historical meteorological dataset, comprising monthly observations from the Station and P CHIRPS3, was stratified into two 20-year periods to enable temporal comparison: Period 1 (P1: 1980–1999) and Period 2 (P2: 2005–2024). A five-year gap (2000–2004) separates P1 and P2, ensuring an equal sample size ($n = 270$ in each period) with a comparable statistical power. The 20-year periods capture long-term trends rather than short-term variability, consistent with climate change detection methodologies employed in regional climate studies [24]. We used the two-sample Student's t -test with the null hypothesis H_0 that the means of two independent populations (Periods 1 and 2) were equal. Statistical significance was evaluated at three levels: $\alpha = 0.05$ (*), indicating moderate evidence; $\alpha = 0.01$ (**), indicating strong evidence; and $\alpha = 0.001$ (***), indicating very strong evidence against H_0 . This procedure follows common practices in statistical climatology studies. The analysis and data visualization were performed using violin boxplots, a hybrid graphical method that combines kernel density estimation with traditional box-and-whisker plots to provide comprehensive distributional information. The method generates a smoothed probability density function for each dataset, which is then mirrored symmetrically around a central axis to create a characteristic violin shape. This approach allows for the simultaneous visualization of data distribution shape, central tendency measures, and variability patterns. Within each violin, traditional boxplot elements were superimposed, including the median (central line), first and third quartiles (box boundaries), and outliers (individual points

beyond 1.5 times the interquartile range). For each variable, separate violin plots were constructed for the four temporal–seasonal combinations: P1-Dry, P1-Wet, P2-Dry, and P2-Wet, enabling direct visual comparison of distributional changes across both temporal periods and seasonal regimes.

The final part of this work is the analysis of extreme seasonal climate events, based on statistical comparison of the relative frequency and magnitude of extreme events between the two 20-year periods, P1 (1980 to 1999) and P2 (2005 to 2024). Extreme events were defined using the percentile-based approach recommended by the WMO and widely adopted in climate extremes research [25,26]. For each meteorological variable, the 10th (P10) and 90th (P90) percentile thresholds were calculated separately for each period–season combination to account for both temporal and seasonal variations in the historical series from 1980 to 2024. An observation x_i for meteorological variable X in period p (P1 and P2) and season s (Wet and Dry) was classified as an extreme event if

$$\text{Low Extreme: } x_i \leq P10(X,p,s) \quad (8)$$

$$\text{High Extreme: } x_i \geq P90(X,p,s) \quad (9)$$

The relative frequency RF in % of extreme events was calculated for each combination of variable, extreme type e (Low or High extreme), period p , and season s using

$$RF(X,e,p,s) = [N_extreme(X,e,p,s)/N_total(p,s)] \times 100 \quad (10)$$

where $N_extreme$ = number of extreme events of type e , and N_total = total number of observations in period p and season s .

The magnitude of Low and High extremes was quantified by averaging all selected events in each variable, period, and season, providing insight into the intensity of extreme conditions. Thus, the absolute and relative changes between P1 and P2 were plotted in a scatter diagram showing the RF on the x-axis and the magnitude on the y-axis. As mentioned, this Amazon region has a unique meteorological station with complete historical data from 1980 onwards, so this approach assumes that the 20-year periods provide sufficient temporal resolution to capture meaningful climate variability while minimizing the influence of short-term fluctuations.

3. Results

3.1. Annual Climatological Cycle, Seasonal Regimes, and Spatial Configuration of Precipitation

Figure 2 displays the climatological normals (1991–2020) for the surface conventional station in Belém, summarizing the annual cycle of all meteorological variables in a comprehensive climatological meteogram. Based on the annual cycle of P , the most critical variable for characterizing tropical climates [27], it is possible to distinguish the Wet (December to May) and Dry (June to November) regimes, defined by precipitation levels above and below the annual mean of 276 mm, respectively. Belém exhibits a well-defined unimodal seasonal structure with six months in each regime. The Wet season begins in December (283 mm), peaks in March (513 mm), and concludes in May (324 mm). This period is marked by high atmospheric moisture (RH ranging from 83.7% to 89.5%), low thermal amplitude (TN from 23 to 23.4 °C and TX from 30.9 to 32.5 °C), and relatively calm wind conditions (WS between 1.1 and 1.5 m s^{−1}). Conversely, the Dry season starts in June (206 mm), reaches minimum precipitation in August and September (129 mm and 120 mm), and ends in November (151 mm). This regime is characterized by reduced humidity (RH between 79.3% and 82.8%), higher thermal amplitude (TN from 22.8 to 23.1 °C; TX from 32.5 to 33.2 °C), and stronger wind activity (WS between 1.5 and 1.9 m s^{−1}).

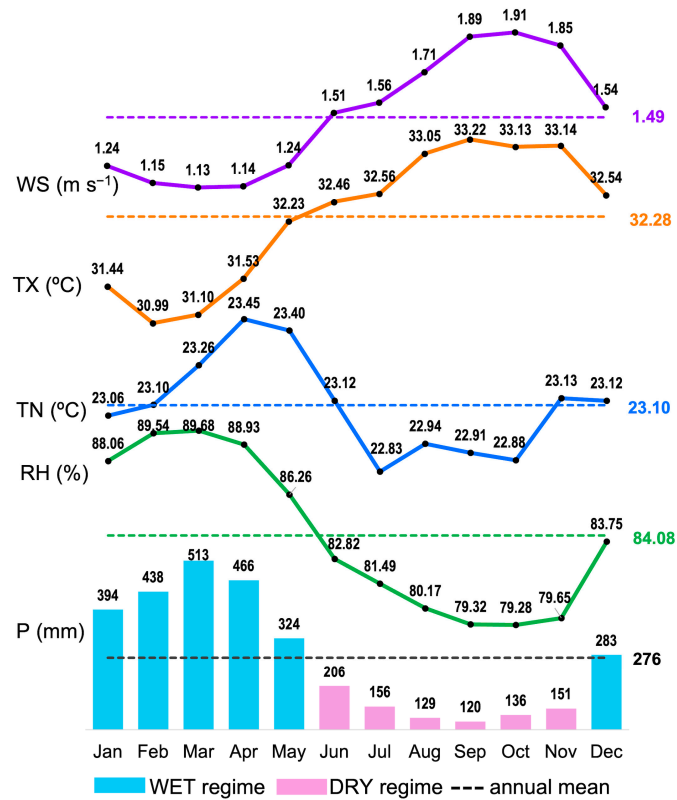


Figure 2. Climatological meteogram for the INMET station in Belém with climatology (1991 to 2020) of P Station (mm), TN (°C), TX (°C), RH (%), and WS (m s^{−1}). The dashed lines indicate the annual means, with the values to the right. The colors in the P bars indicate the seasonal regimes.

Table 1 presents the descriptive statistics of complete meteorological variables for Belém station, and also for P CHIRPS3. Figure A1 (see Appendix A) illustrates boxplots for the entire data series, from 1980 to 2024. The circle and square symbols show the annual means for each variable and seasonal regime, in which pronounced variability and signs of trends are observed. These aspects are discussed in further detail in subsequent sections.

Table 1. Descriptive statistics considering the climatological normal (1991 to 2020) of all variables at the Belém station for the Wet and Dry regimes. The P10 and P90 percentile values were calculated for the entire series (1980 to 2024) to be used in the extremes analysis item.

Regime	Variable	Min	Q1	Mean	Median	Q3	Max	Coef. Var.	P10	P90
Wet	P Station (mm)	103.3	299.1	392.6	393.2	464.7	934.0	33.3	222.3	564.4
	P CHIRPS3 (mm)	60.0	305.0	400.9	407.5	496.0	703.5	34.8	239.9	552.1
	TX (°C)	29.30	30.80	31.56	31.60	32.30	34.30	3.21	30.20	32.90
	TN (°C)	21.10	22.80	23.05	23.10	23.40	24.80	2.46	22.30	23.70
	RH (%)	77.90	86.53	88.68	89.10	90.80	95.86	3.58	84.60	92.23
	WS (m s ^{−1})	0.40	0.90	1.20	1.20	1.50	2.40	32.58	0.70	1.70
Dry	P Station (mm)	8.2	101.9	149.7	139.1	188.7	402.0	47.2	67.2	243.3
	P CHIRPS3 (mm)	10.5	110.4	155.3	143.3	190.4	495.0	49.5	72.6	258.5
	TX (°C)	30.90	32.00	32.81	32.70	33.50	35.30	2.88	31.70	34.10
	TN (°C)	20.90	22.33	22.75	22.80	23.20	24.20	2.98	21.80	23.60
	RH (%)	73.30	79.10	81.63	81.55	84.08	89.40	4.02	77.30	86.10
	WS (m s ^{−1})	0.70	1.38	1.67	1.70	2.00	2.80	24.79	1.19	2.20

The scatterplot (Figure 3, left) comparing P Station and P CHIRPS3, based on monthly data for the Wet and Dry regimes from 1980 to 2024, reveals a strong correlation r between these variables, with $R^2 = 0.72$ and $r = 0.85$ for the Wet regime, and $R^2 = 0.74$ and $r = 0.86$ for the Dry regime. These results support the utility of CHIRPS3 for analyzing spatial precipitation patterns at the municipal scale in the Belém and adjacent cities. The climatological map

(1991–2020) of P CHIRPS3 in Figure 3 highlights a precipitation maximum (160 to 175 mm) over Mosqueiro Island (northern region). A secondary area of slightly lower precipitation (155 to 160 mm) is evident in the southern portions of the municipalities BE, AN, and MA. During the Wet regime, this spatial pattern reverses, with the highest precipitation (370 to 400 mm) occurring in the southern portion of the region, encompassing most of the continental territories of BE, AN, and MA. At the geographic location of the meteorological station (denoted by a circle on the maps), CHIRPS3 estimates approximately 155 mm for the Dry and 400 mm for the Wet regime, closely aligning with the Station's climatological values (Table 1: 150 mm for Dry, 393 mm for Wet).

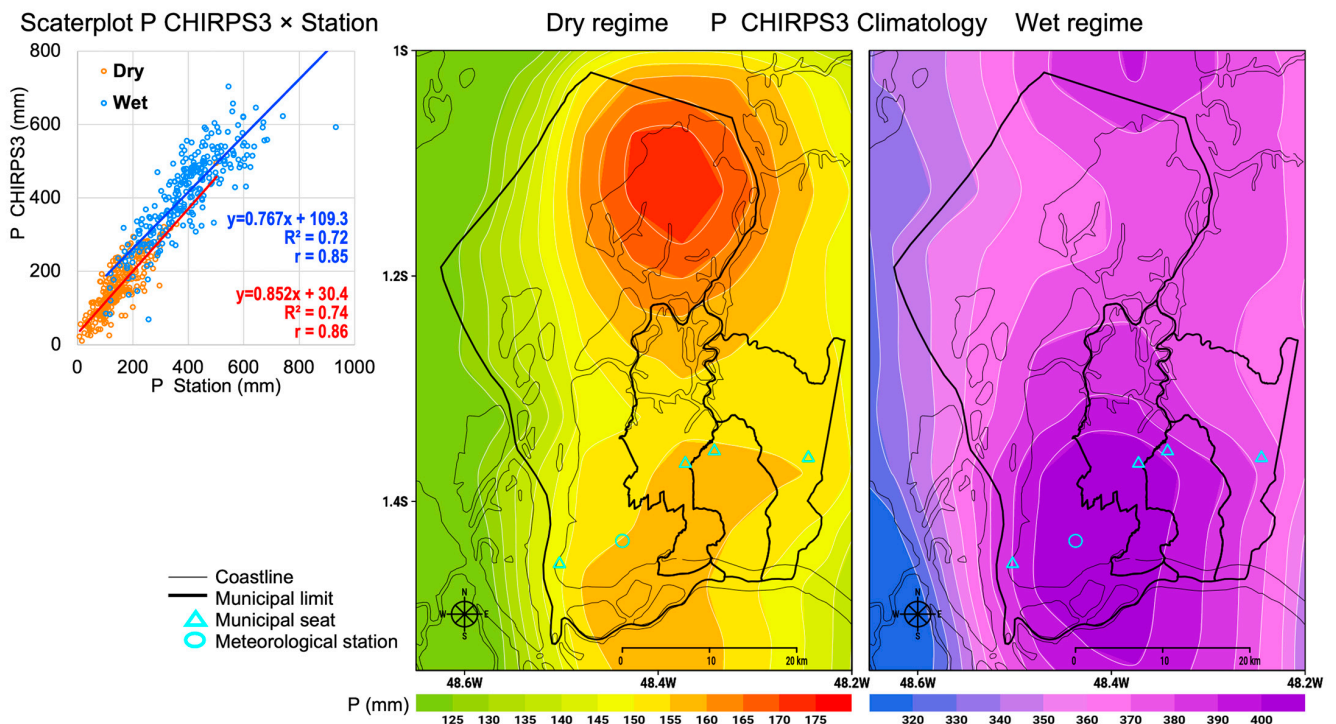


Figure 3. P Station and P CHIRPS3 scatterplot for monthly data in the Wet and Dry regimes from 1980 to 2024 (left); spatial patterns of CHIRPS3 climatology (1981–2024) in the Wet and Dry regimes.

3.2. Environmental Changes Given by Satellite Mapping of LULC

Figure 4 documents four decades of environmental transformations, primarily driven by human-induced land-use activities, across an area encompassing the municipalities of BE, AN, MA, and BN. In 1985, the LULC map indicates substantial Urban areas in the southern part of BE, with scattered patches in its central and northern sections, as well as in central AN (already conurbated with BE) and in smaller sectors of MA and BN with an urbanization sparse. Forest cover was dominant in the southeastern part and islands north of BE (Caratateua and Mosqueiro, excluding its coastal Urban strip), the extreme north and south of AN, and much of MA and BN. In the percentage distribution of LULC classes, the pie chart for 1985 (Figure 4, bottom left) shows Forest occupying approximately 45.6%, followed by Water at 39%. Urban areas comprised nearly 9%, with Pasture and Grassland at about 5.1% and 1.4%, respectively. By 2023, Urban expansion had encompassed all of central and northern BE, most of Caratateua Island, and the entire coastal zone of Mosqueiro Island. Urbanization also intensified in the central-northern parts of AN and MA and around BN's municipal seat and its northern section. Pasture areas expanded, largely at the expense of forest, particularly in BN and inland Mosqueiro. The 2023 LULC map reveals a nearly continuous urban sprawl of ~30 km (see km scale ruler at the base of the map), indicating a consolidated conurbation across the four municipalities.

The updated pie chart shows Forest reduced to 36.3%, Water relatively stable at 38.7%, while Urban and Pasture expanded to 16.4% and 8.5%, respectively. Grassland was nearly eliminated. Thus, in terms of total area over the full period (1985 to 2023), Forest declined by 9.29%, Grassland by 1.31%, and Water by 0.25%, while Urban and Pasture increased by 7.48% and 3.37%, respectively. Figure 4 (bottom right) presents the 1985 to 2023 time series of annual LULC evolution, and the arrows on the right emphasize the variations in each class individually over the period. With some small annual oscillations, Forest area decreased from 70,261 to 55,948 ha (~20.4% loss). The systematically increasing trend of Urban area is evident, increasing from 13,766 to 25,288 ha (~83.7% gain), and Pasture also rose from 7919 to 13,118 ha (~65.6% gain). With lower values compared to other LULC classes, Grassland declined sharply from 2105 to just 89 ha (~96% loss), and the Water curve shows stable annual variation with a slight decrease (~0.65%).

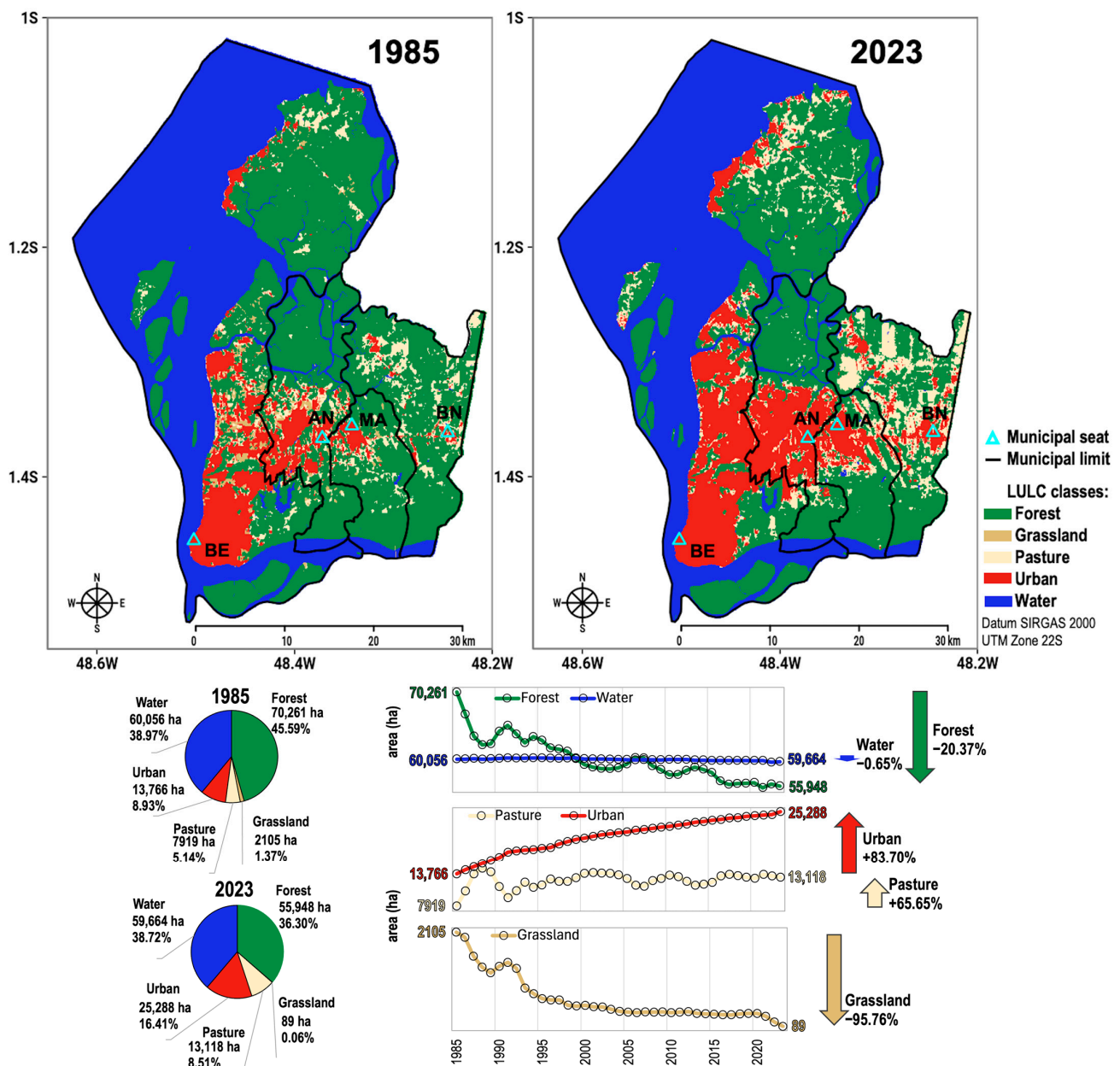


Figure 4. Top panel: LULC maps for 1985 and 2023. Bottom panel: pie-charts with area (ha) and respective percentages for 1985 and 2023 (**left**) and time series of annual area (ha) in each LULC class from 1985 to 2023 (**right**), with arrows indicating the individual variation in the period.

3.3. Long-Term Trends

Given the minimal variability in the Water class and the limited extent of Grassland cover, only the Forest, Urban, and Pasture LULC classes and all station meteorological variables (by season) were retained for trend analysis over the 1985–2023 period.

Figure 5 shows the original data (points) and the Sen slope trend lines, with Table 2 indicating the quantitative results obtained from Mann–Kendall tests. For the Wet regime, statistically significant monotonically increasing trends were found for TX and TN (Tau > 0; p -value < 0.001), along with P (p -value < 0.01). Wind speed (WS) showed a significant negative trend (p -value < 0.001), while RH did not exhibit a significant trend. In the Dry regime, all variables except P showed significant trends: TX and TN increased (Tau > 0), while RH and WS declined (Tau < 0). Likewise, environmental variables revealed strong statistical trends: Urban area showed a significant increasing trend (positive Tau, p -value < 0.001), Forest showed a significant decreasing trend (negative Tau, p -value < 0.001), while Pasture displayed a non-significant positive trend.

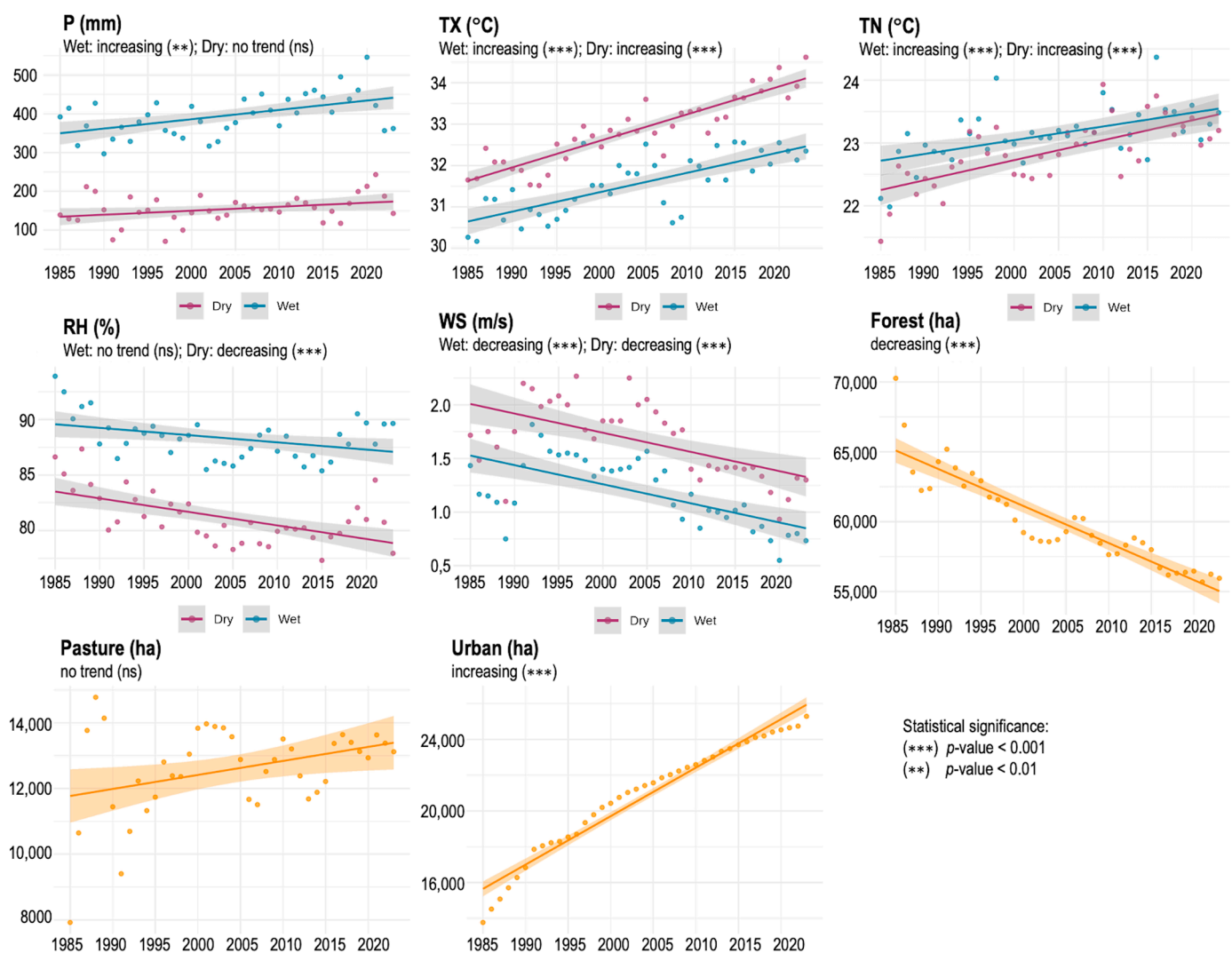


Figure 5. Mann–Kendall test for 1985–2023 time series for P Station (mm), TX (°C), TN (°C), RH (%), and WS (m s^{-1}) during Wet and Dry regimes and annual Forest (ha), Pasture (ha), and Urban (ha) areas. The points represent the original data, solid lines represent Sen's slope trends, and the shaded bands show the 95% confidence intervals. The text below each variable indicates the interpretation of the trend results with statistical significance.

Table 2. Quantitative results obtained in the Mann–Kendall test and Sen’s slope trend for the climate and environmental variables during the Wet and Dry regimes, from 1983 to 2023.

Regime	Variable	Tau	Trend	CI Lower	CI Upper	p-Value
Wet	P Station (mm)	3.24	2.5 mm yr ^{−1}	1.0	4.1	0.001
	TX (°C)	4.84	0.05 °C yr ^{−1}	0.04	0.06	<0.001
	TN (°C)	3.79	0.02 °C yr ^{−1}	0.01	0.03	<0.001
	RH (%)	−1.83	−0.06% yr ^{−1}	−0.13	0.01	0.068
	WS (m s ^{−1})	−4.66	−0.02 m s ^{−1} yr ^{−1}	−0.03	−0.01	<0.001
Dry	P Station (mm)	1.96	1.01 mm yr ^{−1}	−0.02	2.02	0.050
	TX (°C)	6.69	0.07 °C yr ^{−1}	0.05	0.08	<0.001
	TN (°C)	4.36	0.03 °C yr ^{−1}	0.02	0.04	<0.001
	RH (%)	−3.48	−0.13% yr ^{−1}	−0.18	−0.06	<0.001
	WS (m s ^{−1})	−3.86	−0.02 m s ^{−1} yr ^{−1}	−0.03	−0.01	<0.001
Annual	Forest (ha)	−7.26	−246.8 ha yr ^{−1}	−283.5	−208.6	<0.001
	Pasture (ha)	1.69	36.4 ha yr ^{−1}	−7.1	72.9	0.090
	Urban (ha)	8.95	246.9 ha yr ^{−1}	223.1	271.6	<0.001

3.4. Correlations and PCA Analyses

The quantitative results in Table 3 and a complete correlogram with the results for all available pairs of variables are shown in Figure 6. However, the focus of this work was on investigating the effect or impact of environmental transformations (given by LULC changes) on the seasonal behavior of climate variables, whose results are emphasized by the circles and rectangles in Figure 6. Table 3 and Figure 6 exhibit statistically significant correlations between Forest and TX (−0.87 for Dry and −0.77 for Wet), Forest and TN (−0.73 for Dry and −0.61 for Wet), Forest and RH (0.59 for Dry), and Forest and WS (0.56 for Wet), as well as correlations between Urban and TX (0.87 for Dry and 0.75 for Wet), Urban and TN (0.72 for Dry and 0.60 for Wet), Urban and RH (−0.68 for Dry and −0.51 for Wet), and Urban and WS (0.52 for Wet). These results demonstrate that the metropolitan region of Belém experienced a suppression of forest cover in conjunction with the expansion of densely urbanized areas, which are strongly correlated with systematic increases in the maximum and minimum air temperatures in both seasonal regimes. The Dry season shows generally stronger correlations than the Wet season, suggesting heightened climate–environment interactions under water-limited conditions.

Table 3. Correlations between variable pairs for Wet and Dry seasons from 1985 to 2023.

Variable Pair	Regime	Correlation	p-Value	Regime	Correlation	p-Value
Forest vs. P Station	Wet	−0.39	0.015	Dry	−0.36	0.026
Forest vs. TX		−0.77	<0.001		−0.87	<0.001
Forest vs. TN		−0.61	<0.001		−0.73	<0.001
Forest vs. RH		0.47	0.002		0.59	<0.001
Forest vs. WS		0.56	<0.001		0.49	0.002
Pasture vs. P Station		0.04	0.791		0.40	0.012
Pasture vs. TX		0.47	0.003		0.48	0.002
Pasture vs. TN		0.39	0.015		0.43	0.006
Pasture vs. RH		−0.20	0.221		−0.14	0.403
Pasture vs. WS		−0.35	0.030		−0.29	0.072
Urban vs. P		0.46	0.003		0.26	0.110
Urban vs. TX		0.75	<0.001		0.87	<0.001
Urban vs. TN		0.60	<0.001		0.72	<0.001
Urban vs. RH		−0.51	0.001		−0.68	<0.001
Urban vs. WS		−0.52	0.001		−0.46	0.003

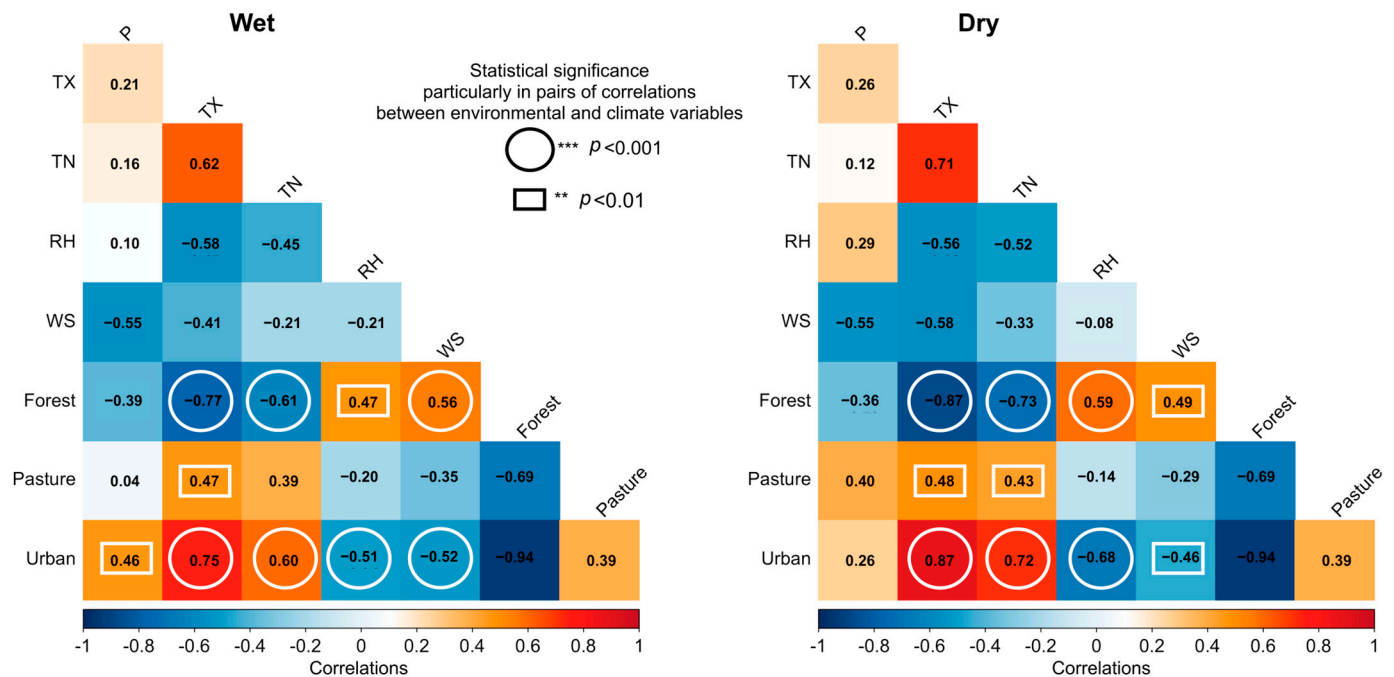


Figure 6. Correlogram between environmental (LULC classes of Forest, Pasture, and Urban) and climate (P Station, TX, TN, RH, and WS) variables for Wet and Dry regimes from 1985 to 2023. Circle and rectangle symbols emphasize statistical significance, particularly in pairs of correlations between environmental and climate variables.

Complementing the analyses, Table 4 depicts the quantitative results of the PCA analysis and Figure 7 displays PCA biplots to help in interpreting the interactions between the environmental and climate variables. This multivariate technique revealed relevant patterns for the period 1985–2023 with the identification of two significant principal components (eigenvalues > 1.0) for both seasons, explaining 73% and 78% of total variance for the Wet and Dry regimes, respectively. In the Wet regime, PC1 explains 53.1% and PC2 explains 19.9% of the variance, while in the Dry regime, PC1 explains 56.8% and PC2 explains 21.1% of the variance. In the PCA biplot, PC1 represents a clear environmental gradient, with Forest cover loading negatively (-0.47 in Wet, -0.46 in Dry) and Urban areas loading positively (0.45 in Wet, 0.44 in Dry), indicating an urbanization–deforestation axis. Air temperature variables (TX, TN) consistently loaded positively on PC1, suggesting their direct association with Urban expansion effects. Seasonal differences were evident in the PC1 variance explanation, with the Dry regime showing higher explanatory power (56.8%) compared to the Wet regime (53.1%), indicating stronger environmental–climate coupling during periods of water stress in tropical urban regions. The Kaiser criterion validated the significance of the first two components. The most important interpretation highlighted in this analysis was the clear and robust separation between the Forest and Pasture/Urban variables, thus confirming the dominant role of land use in regional climate modulation. The similar quadrant patterns between the two regimes suggest consistent land-use–climate relationships, though with varying intensities reflecting seasonal atmospheric dynamics in the region.

Table 4. PCA analysis was applied to climate and environmental variables for the Wet and Dry regimes in the period from 1985 to 2023.

Statistics	Regime	Items and Variables	PC1	PC2	PC3	PC4	PC5	PC6	PC7
Variance explained	Wet	Std. deviation	2.06	1.26	0.93	0.70	0.63	0.49	0.39
		Proportion variance	0.53	0.20	0.11	0.06	0.05	0.03	0.02
		Cumulative proportion	0.53	0.73	0.84	0.90	0.95	0.98	1.00
	Dry	Std. deviation	2.13	1.30	0.87	0.65	0.59	0.37	0.34
		Proportion variance	0.57	0.21	0.09	0.05	0.04	0.02	0.01
		Cumulative proportion	0.57	0.78	0.87	0.93	0.97	0.99	1.00
PCA loadings	Wet	Forest	−0.47	−0.02	0.11	−0.18	0.10	−0.35	−0.18
		Pasture	0.30	−0.04	−0.77	0.11	−0.43	−0.18	−0.05
		Urban	0.45	0.03	0.24	0.16	0.06	0.54	0.28
		P Station	0.21	0.55	0.46	0.02	−0.57	−0.35	0.00
		TX	0.42	−0.15	0.05	0.06	0.45	−0.65	0.42
		TN	0.35	−0.22	0.06	−0.89	−0.09	0.05	−0.15
		RH	−0.26	0.57	−0.31	−0.36	0.11	0.11	0.60
		WS	−0.28	−0.56	0.15	−0.01	−0.51	−0.02	0.58
	Dry	Forest	−0.46	−0.01	−0.14	0.16	−0.10	0.13	0.40
		Pasture	0.29	−0.22	0.79	0.18	0.31	0.14	0.04
		Urban	0.44	0.13	−0.19	−0.30	−0.05	−0.23	−0.50
		P Station	0.17	−0.62	0.03	−0.54	−0.45	0.14	0.26
		TX	0.44	0.04	−0.18	0.08	0.22	−0.55	0.64
		TN	0.38	0.15	0.03	0.57	−0.70	0.13	0.02
		RH	−0.28	−0.56	0.03	0.35	−0.10	−0.62	−0.30
		WS	−0.27	0.45	0.53	−0.33	−0.37	−0.44	0.10

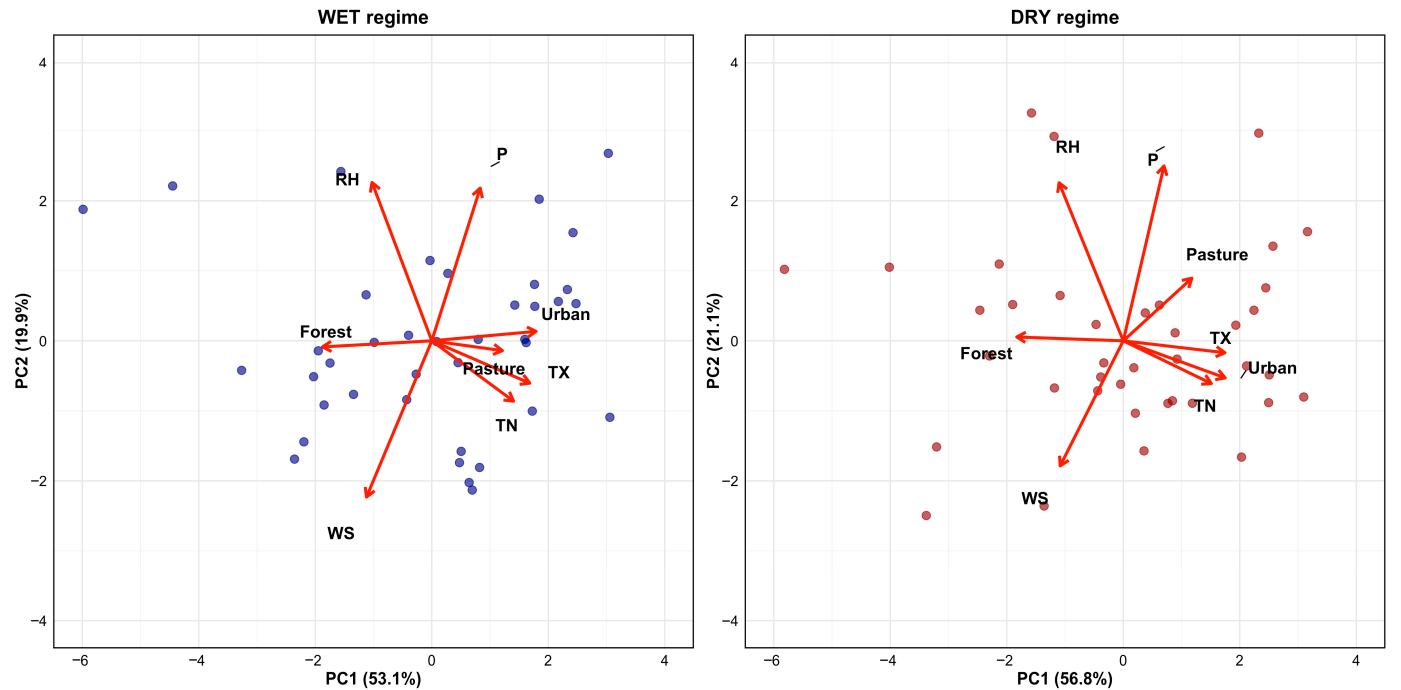


Figure 7. PCA biplot between environmental (LULC classes of Forest, Pasture, and Urban areas) and climate (P Station, TX, TN, RH, and WS) variables for the Wet and Dry regimes in the period from 1985 to 2023.

3.5. Differences Between Past and Present Decades

To quantify the most significant shifts in regional climate, the data were split into two 20-year periods: P1 (1980–1999) and P2 (2005–2024). The quantitative results in Table 5 and the violin boxplot analysis in Figure 8 reveal significant distributional changes in climate variables between the two study periods across both the Dry and Wet regimes. Air temperature variables (TX and TN) exhibit clear distributional shifts toward higher values in P2, with TX showing a pronounced increase of 1.47 ± 0.17 °C during the Dry season and 0.98 ± 0.24 °C during the Wet season ($p < 0.001$), while TN increased by 0.89 ± 0.14 °C and 0.54 ± 0.14 °C, respectively ($p < 0.001$). The boxplots demonstrate that these temperature changes were accompanied by relatively maintained distributional shapes, suggesting a systematic warming trend rather than increased variability. Conversely, RH distributions show a notable leftward shift in P2, with mean reductions of $3.91 \pm 0.69\%$ (Dry) and $2.15 \pm 0.75\%$ (Wet) ($p < 0.001$), while maintaining their characteristic near-normal distributions. WS exhibited the most dramatic distributional changes, with highly skewed distributions in both periods showing significant reductions in P2 (0.40 ± 0.09 m s^{−1} for the Dry regime and 0.44 ± 0.09 m s^{−1} for the Wet regime ($p < 0.001$), indicating a systematic weakening of regional wind patterns. Precipitation variables display characteristic right-skewed distributions typical of rainfall data, with Station measurements showing ($p < 0.001$) significant increases of 18.7% or 25.7 ± 18.5 mm (Dry) and 18.4% or 66.9 ± 32.6 mm (Wet), while CHIRPS3 satellite data revealed more modest increases of 12.3% or 18.4 ± 18.1 mm (Dry) and 8.5% or 34.1 ± 29.3 mm (Wet).

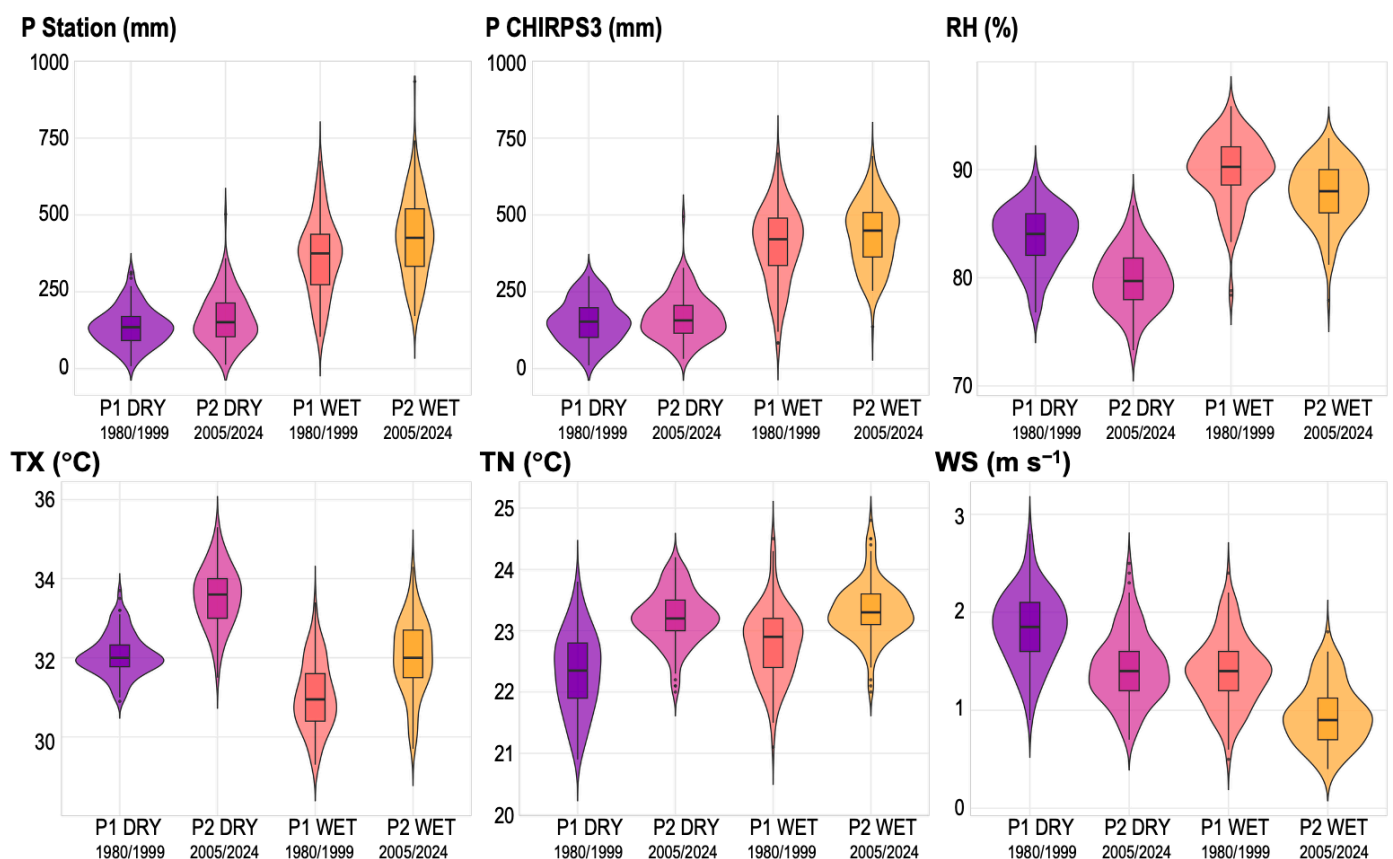


Figure 8. Violin boxplots of for P Station (mm), P CHIRPS3 (mm), TX (°C), TN (°C), RH (%), and WS (m s^{−1}) in the Wet and Dry regimes for the 20-yr periods P1 (1980 to 1999) and P2 (2005 to 2024). Bold text indicates the magnitude of changes between the two periods.

Table 5. Quantitative results of the means calculated in the 20-yr periods P1 (1980 to 1999) and P2 (2005 to 2024), including absolute and percentage changes, uncertainty (standard deviation), confidence interval, and statistical significance.

Regime	Variable	P1 Mean	P2 Mean	Abs. Change	% Change	Uncertainty	Confidence Int.	p-Value
Wet	P Station (mm)	364.4	431.3	66.9	18.4	±32.6	34.2 to 99.5	0.001
	P CHIRPS3 (mm)	400.3	434.4	34.1	8.5	±29.3	1.8 to 60.3	0.040
	TX (°C)	31.05	32.03	0.98		±0.24	0.75 to 1.22	<0.001
	TN (°C)	22.79	23.33	0.54		±0.14	0.40 to 0.67	<0.001
	RH (%)	89.94	87.79	−2.15		±0.75	−2.90 to −1.40	<0.001
	WS (m s ^{−1})	1.40	0.96	−0.44		±0.09	−0.52 to −0.35	0.001
Dry	P Station (mm)	137.1	162.8	25.7	18.7	±18.5	7.3 to 44.2	0.006
	P CHIRPS3 (mm)	149.9	168.3	18.4	12.3	±18.1	−2.6 to 33.5	0.037
	TX (°C)	32.08	33.54	1.47		±0.17	1.30 to 1.64	<0.001
	TN (°C)	22.33	23.22	0.89		±0.14	0.75 to 1.03	<0.001
	RH (%)	83.77	79.86	−3.91		±0.69	−4.60 to −3.22	<0.001
	WS (m s ^{−1})	1.84	1.44	−0.40		±0.09	−0.49 to −0.31	<0.001

3.6. Changes in Extreme Events: Point Analysis in Belém and Spatial Distribution of P CHIRPS3

This final analysis assesses whether seasonal extreme events have intensified over the past four decades. The scatterplots for P Station in Figure 9 show the quantitative values of the relative frequency (x-axis) and magnitude (y-axis) for Low and High extremes in periods P1 and P2, with arrows indicating the direction of change. Key findings include the following:

- For the P variable, the relative frequency for High extremes increased by 4.5% in the Wet season and 4% in the Dry season, with respective magnitude increases of 23 mm and 16 mm. Low extremes declined in frequency in the Wet season (−4%) but intensified by 33 mm; the Dry season showed a slight frequency rise (0.8%), while magnitude decreased by −2 mm.
- TX High extremes surged in frequency and magnitude during both regimes (+7% and +0.2 °C in Wet; +10% and +0.4 °C in Dry). Low extremes dropped sharply in frequency, with −6% in Wet and −10% in Dry, accompanied by weaker intensification in magnitude of about +0.1 °C in both regimes.
- For the High extremes, TN amplified the frequency by about +6% in the Wet (with a retraction in the magnitude of −0.1 °C) and +9% in the Dry (without changes in magnitude). The relative frequency of TN in the Low extreme reduced strongly by −10% in the Dry regime and by −9% in the Wet regime, with a magnitude increase of 0.1 °C in the Wet regime and no change in the Dry regime.
- RH High extremes decreased by −0.5 to −1% in intensity and −9% in relative frequency in both seasons. Low extremes increased in frequency by +9% in the Wet regime and +7% in the Dry regime, with a −1.4% drop in intensity in the Wet regime and −1% in the Dry regime.
- WS High extremes decreased in relative frequency (−7% in Wet, −9% in Dry) and magnitude (−0.1 m s^{−1} in Wet). For the Low extremes, frequency increased (8% in Wet, 10% in Dry) with stable magnitudes.

Similar to the results described for the P Station variable, the P CHIRPS3 maps in Figure 10 illustrate the spatial distribution (at grid points) of changes in the relative frequency and magnitude of High and Low precipitation extremes across the geographic domain encompassing Belém and its surrounding metropolitan municipalities, comparing the two periods (P2 and P1).

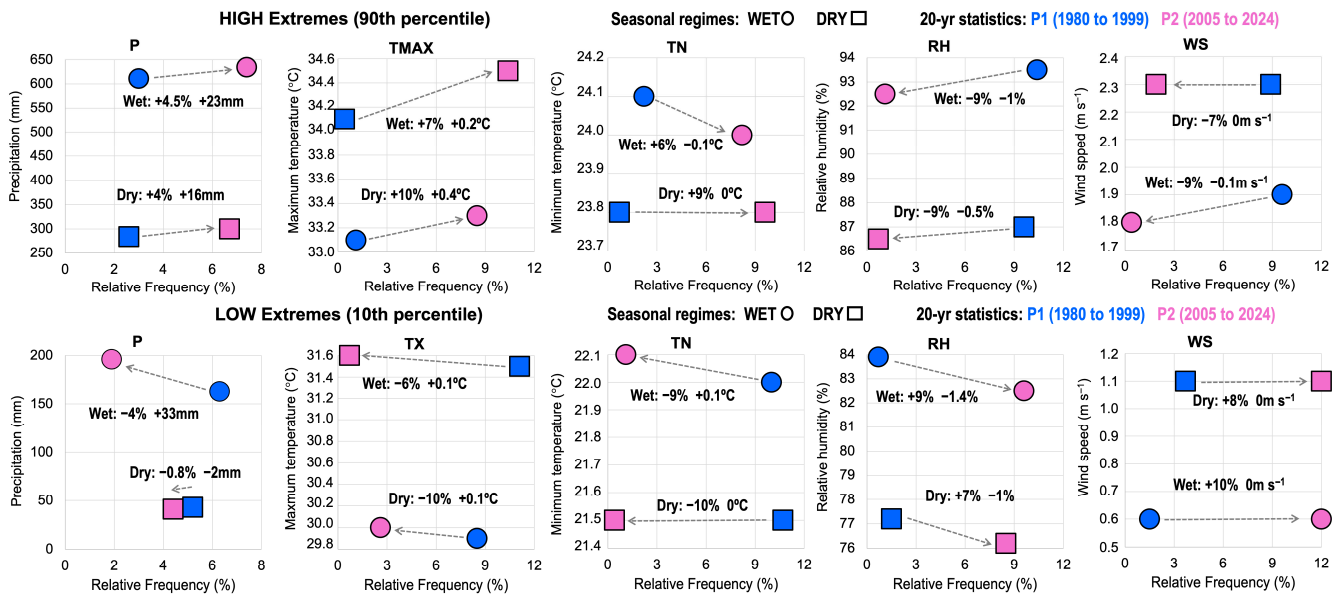


Figure 9. Scatterplot of the relative frequency and magnitude of High (top) and Low (bottom) extreme seasonal events for the 20-yr periods P1 (1980 to 1999) and P2 (2005 to 2024) in Wet and Dry regimes. Arrows and bold text indicate the direction and quantitative values of changes.

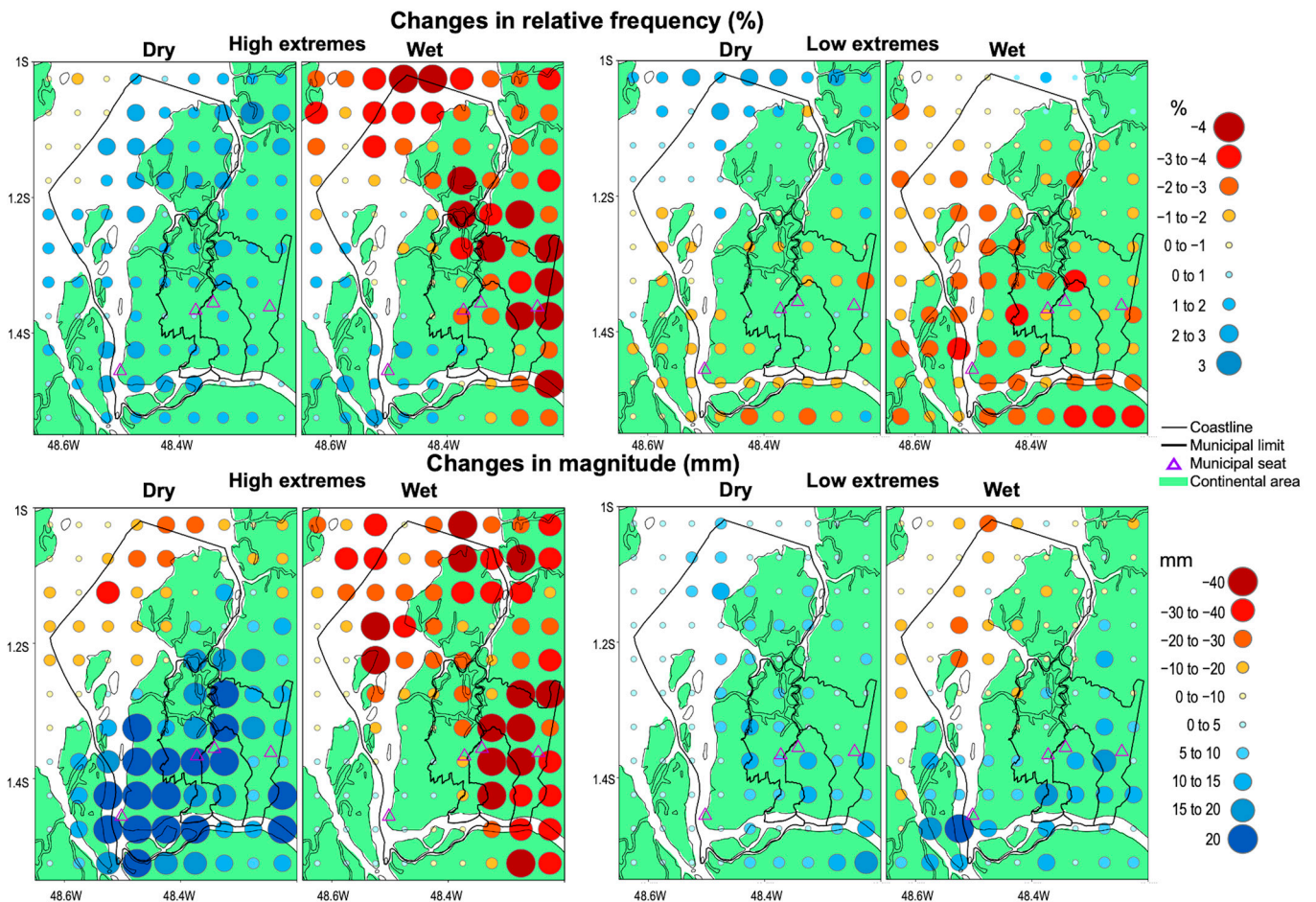


Figure 10. P CHIRPS3 changes in the relative frequency (%) and magnitude (mm) of High and Low extremes between periods P2 and P1 for Wet and Dry regimes along the metropolitan region of Belém and neighboring municipalities.

For High extremes during the Dry season, an overall amplification in frequency is evident throughout the region, accompanied by a marked intensification in precipitation magnitude. The most pronounced increases up to 20 mm are concentrated over the continental areas of Belém, Ananindeua, and Marituba. In contrast, the Wet season exhibits a more heterogeneous spatial pattern: a localized increase in frequency (ranging from 1% to 3%) is restricted to the southern portion of Belém, while widespread reductions in frequency are observed across the western, central, and northern sectors of the study area. The decrease in magnitude is modest in the southern continental area of Belém (0–10 mm), but becomes substantially more severe elsewhere, with reductions reaching −30 to −40 mm (Figure 10, left panel).

For Low extremes in the Dry regime, most of the continental region (excluding the northernmost area, including Mosqueiro Island) shows evidence of a slight decrease in frequency (−1% to −2%), along with an increase in precipitation magnitude of approximately 5 to 15 mm. During the Wet regime, a similar trend is observed, with a more widespread increase in frequency (1% to 4%) and intensification of magnitudes ranging from 5 to 20 mm across all municipalities. The only exception is Mosqueiro Island, where a localized reduction in precipitation magnitude is noted (Figure 10, right panel).

4. Discussion

The integrated analysis of LULC changes, long-term climate trends, and seasonal extreme event evaluations over the past four decades provides a comprehensive understanding of climate–environment interactions in a densely populated and conurbated metropolitan region that extends over 30 km across four municipalities (Belém, Ananindeua, Marituba, and Benevides) within eastern Brazilian Amazon. Our findings reveal significant shifts in both climate and environmental variables, with strong interdependencies between urbanization, suppression of forest cover (deforestation), and local meteorological conditions. Notably, the inclusion of relative humidity and wind speed alongside traditional variables (precipitation and surface air temperature) offers novel insights into the regional climate alterations induced by land-use changes, an aspect underexplored in prior Amazonian studies. Furthermore, the incorporation of the updated version of satellite-derived precipitation data (CHIRPS3) complements in situ observations, enhancing the spatial resolution and robustness of our findings. Trend analyses and comparison between past (1980–1999) and current (2005–2024) decades evidence a marked increase in precipitation in both Station and CHIRPS3 satellite data, and a systematic atmospheric warming of 1–1.5 °C in maximum air temperature (TX) and 0.5–0.9 °C in minimum air temperature (TN) in both seasonal regimes, alongside declines in wind speed (0.4–0.44 m s^{−1}) and relative humidity (2–4%) particularly in the Dry season. These trends align with extensive LULC changes (1985 to 2023), where Forest cover declined by ~20%, while Urban and Pasture areas expanded by ~84% and 65%, respectively, suggesting a strong anthropogenic influence on local climate conditions. Correlation and PCA analyses revealed robust associations and co-variability between LULC changes and climate variables. In the Dry regime, Forest loss correlates strongly with rising temperatures ($r = -0.87$ for TX) and declining RH ($r = 0.59$), whereas urbanization correlates positively with air temperature ($r = 0.87$ for TX) and negatively with RH ($r = -0.68$). The PCA further underscores an urbanization–deforestation gradient, with stronger climate–environment coupling in the Dry season, likely due to reduced moisture availability amplifying land surface feedbacks. It is important to note that while these statistical associations are strong and physically plausible, they do not unequivocally prove causation. The observed trends are likely the result of combined global warming and regional LULC changes. However, the strength of the correlations, the consistency across multiple meteorological variables, and the stronger signal in the

Dry season (when local surface–atmosphere feedbacks are dominant) provide compelling evidence that LULC changes are a significant contributor to the observed local climate trends. Likewise, a critical observational finding is the intensification of seasonal extreme events. High precipitation extremes (90th percentile) increased in frequency (4 to 4.5%) and magnitude (16 to 23 mm), while Low extremes (10th percentile) exhibited contrasting trends, with reductions in frequency in the Wet season but magnitude increases in both seasons. Surface air temperature extremes showed even more dramatic shifts, with High extremes becoming 7–10% more frequent and Low extremes declining sharply in frequency (6–10%).

Our findings align with and expand upon prior research on Amazon climate that has documented warming trends and altered precipitation patterns in the region [3,28]. Considering recent studies, Terassi [29] evaluated the indicators of extreme events in the Brazilian Legal Amazon based on historical data from INMET meteorological network, with indications that the eastern portion presents the most pronounced signs of higher temperatures, in agreement with [2,30]. Marengo [5] stated that the warming trend has been more evident since 1980 and has further enhanced since 2000. For the Belém station specifically, Terassi [29] reported robust signals (99.9% significance) of more frequent severe precipitation (trends of 11 mm for R95p and 3.8 mm for R99p) in conjunction with strongly positive trends in hot days and nights (trends of 0.5 °C for TX90p and 0.4 °C for TN90p) and negative trends in cold days and nights (−0.2 °C for TX10p and −0.4 °C for TN10p). Our findings for Belém station showed more regionally pronounced increases of nearly 0.5 to 0.9 for TN (air temperature at dawn/early morning) and of 1 to 1.5 °C for TX (air temperature in the afternoon), suggesting stronger local forcings possibly tied to rapid and intense urban growth and deforestation, which may amplify the underlying global warming trend. Moreover, our study provides a significant extension of prior work by quantifying concurrent shifts in surface wind and relative humidity extremes. The results of intensified atmospheric drying and weaker winds reveal additional mechanistic pathways that may exacerbate heat stress in urban areas, a dimension largely overlooked in prior Amazonian urban climate studies. This combination of warmer, drier, and less ventilated conditions in dense urban areas compounds thermal discomfort and has implications for public health. Nevertheless, various studies have reported an intensification of the hydrological cycle over the Amazon basin. Since 2000, the central and northeastern portions have experienced severe flooding events every four years, as summarized in the review by Marengo [5], which are consistent with the broader climate change trends identified by the IPCC [31]. Based on station data and CHIRPS (version 2) from 1981 to 2018, Cavalcante [32] documented positive trends in the R20mm (very heavy precipitation days) and R95p (total precipitation on days when precipitation > 95th percentile) over the states of Pará and Maranhão in the eastern Amazon. With data up to 2021, Terassi [29] also identified intensified rainfall in several parts of the Amazon, with the Belém station showing significant trends in eight of the eleven extreme rainfall indicators. Investigating the trends in extreme precipitation indicators from CHIRPSv2 for each gridpoint in the Amazon domain, Funatsu [16] detected pronounced spatial variability throughout the basin, with the eastern sector (Belém region in the state of Pará) showing positive coefficients between 2 and 4% for the R20mm and CWD (maximum number of consecutive wet days). Likewise, our satellite-based analysis (CHIRPS3) updated to 2024 reveals finer-scale spatial heterogeneity during the Wet season, contrasting with broader Dry season increases, a pattern not previously resolved in station-only urban climate studies [10]. On the other hand, the strong correlations between LULC changes and surface air temperature trends corroborate the findings by Butt [33], who found that deforestation caused strong warming at distances up to 100 km away from the forest loss areas, while regions experiencing intense urban growth are directly affected by

the excessive increases in minimum and maximum air temperatures [10,34]. A novel insight from our analysis is that urban expansion appears to exert an even stronger influence on the local climate than pasture conversion, as evidenced by the higher PCA loadings for Urban (0.44) versus Pasture (0.21) on the primary component representing the warming trend. This underscores the critical role of the urban heat island effect, driven by changes in thermal properties and surface roughness, as a dominant driver of local climate change in this Amazonian conurbation region. The inclusion of RH and WS data adds mechanistic clarity, i.e., dense urban areas not only heat faster but also become drier and less ventilated, compounding thermal discomfort. The observed decline in wind speed at 10 m, in principle associated with increased surface roughness and urban–canopy effects, is a particularly understudied aspect of Amazonian climate change, which in turn has implications for worsening air pollution in cities. In addition, our detection of RH decrease (−4% in Dry season) and its correlation with suppression of forest cover (deforestation) aligns with the findings of [35], who attributed Amazonian drying to reduced evapotranspiration from forest loss. Future work with complementary approaches using high-resolution meteorological modeling, e.g., Weather Research and Forecasting (WRF) configured for regions of complex orography and environment [36,37] and coupled to urban canopy parameterizations [38], could further investigate and demonstrate the causal mechanisms and feedbacks diagnosed in this observational study and project future climate scenarios under different urban development and deforestation pathways.

5. Conclusions

This study provides an integrated assessment of four decades of environmental and climate changes within the densely populated metropolitan conurbation of the eastern Amazon, centered on Belém (the capital of the state of Pará). Our findings advance the scientific understanding of regional climate change by coupling LULC dynamics with a comprehensive suite of meteorological variables, including previously understudied elements, such as relative humidity (RH) and low-level wind patterns, and CHIRPS v3 satellite-derived precipitation estimates. The analysis reveals that rapid urbanization and concomitant forest loss have driven substantial surface warming (up to 1.5 °C), atmospheric drying (4% decrease in RH), and wind suppression (0.4 m s^{−1} reduction), with particularly pronounced impacts on extreme climate events during the Dry regime.

The results elucidate a critical climate–land-use feedback mechanism, wherein deforestation and urban expansion synergistically intensify regional warming. Particularly alarming is the 7–10% increase in Dry season extreme air temperatures and the emerging spatial heterogeneity in precipitation intensification. These trends collectively exacerbate regional climate extremes, thereby heightening the vulnerability of populations across the urban–peri-urban gradient. The observed patterns of concurrent increases in both High and Low precipitation extremes, coupled with more frequent thermal extremes, align with theoretical frameworks projecting Amazonian tipping points. This suggests that combined thermal stress and moisture deficits could potentially accelerate ecosystem transitions and disrupt regional hydrological cycles [39].

Consequently, our findings call for sustainable development strategies in the Amazon. The evidence base underscores the need for targeted public policies that prioritize the strict conservation of remaining peri-urban forest fragments, which are crucial for moisture recycling and near-surface cooling ecosystem services, particularly within socioeconomically deprived areas. Furthermore, urban planning must strategically integrate green ecological corridors, aligned with prevailing trade winds, to mitigate urban heat island effects and improve air quality. Such integrated planning is imperative for achieving SDG 11 (Sustainable Cities) and SDG 13 (Climate Action). Beyond the local context, this study provides a trans-

ferable framework for investigating land–climate feedbacks in other tropical urbanizing regions. The observed amplification of seasonal climate extremes through synergistic urban and deforestation heating offers critical insight into the potential future of developing cities across the global tropics. Our work underscores the urgent need to incorporate fine-scale LULC dynamics and understudied meteorological variables into climate risk assessments, thereby contributing to a more comprehensive global understanding of anthropogenic climate change.

Author Contributions: Conceptualization, methodology, software, validation, and formal analysis, E.B.d.S.; writing—original draft preparation, E.B.d.S., D.B.d.S.F., A.P.P.d.S., A.C.d.C., J.d.A.S.J., A.M.C.d.C., V.H.d.M.P., T.S.d.S.D., W.P.M.C. and T.A.; writing—review and editing, E.B.d.S., D.B.d.S.F., A.P.P.d.S., A.C.d.C., J.d.A.S.J., A.M.C.d.C., V.H.d.M.P., T.S.d.S.D., W.P.M.C. and T.A.; project administration, E.B.d.S.; funding acquisition, E.B.d.S. and D.B.d.S.F. All authors have read and agreed to the published version of the manuscript.

Funding: This research was partially funded by CNPq (E.B.d.S. 420142/2023-1), and the APC was funded by Instituto Tecnológico Vale.

Data Availability Statement: Databases with respective sources and references are described in the Materials and Methods Section.

Acknowledgments: We thank CNPq for the postdoctoral scholarships (W.P.M.C. 151662/2024-0; T.S.d.S.D. 151674/2024-8) and the Research Productivity Grants provided to E.B.d.S. (314809/2023-6), A.C.d.C. (308302/2025-7), and T.A. (CNPQ—301397/2019-8; FAPESP 2024/00949-5).

Conflicts of Interest: The authors declare no conflict of interest.

Appendix A

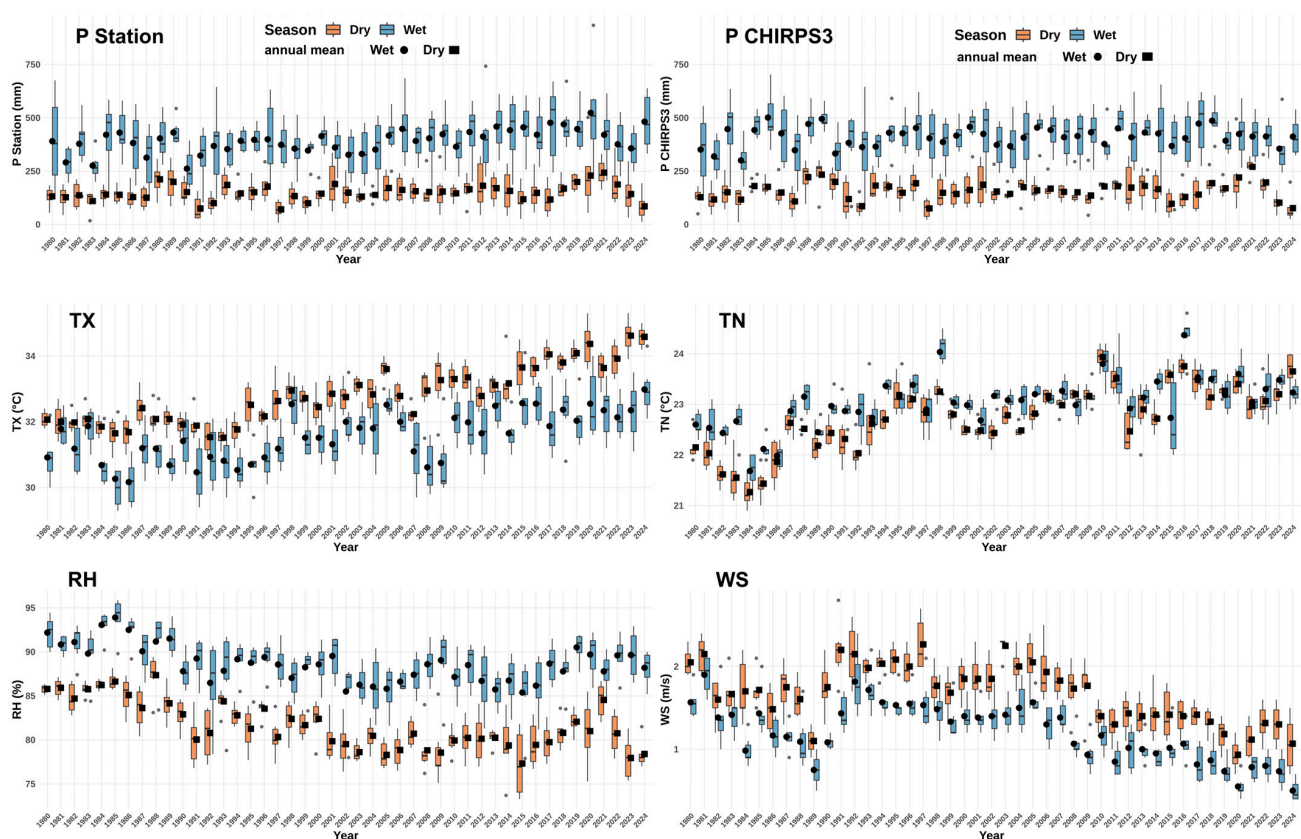


Figure A1. Boxplot of monthly P Station, P CHIRPS3, TX, TN, RH, and WS data in each Wet and Dry regime from 1980 to 2024. Black circle and square symbols show the seasonal means in each year.

References

- Alkama, R.; Cescatti, A. Biophysical climate impacts of recent changes in global forest cover. *Science* **2016**, *351*, 600–604. [CrossRef]
- Davidson, E.; de Araújo, A.; Artaxo, P.; Balch, J.K.; Brown, I.F.; Bustamante, M.M.C.; Coe, M.T.; DeFries, R.S.; Keller, M.; Longo, M.; et al. The Amazon basin in transition. *Nature* **2012**, *481*, 321–328. [CrossRef]
- Marengo, J.A.; Souza, C.M., Jr.; Thonicke, K.; Burton, C.; Halladay, K.; Betts, R.A.; Alves, L.M.; Soares, W.R. Changes in climate and land use over the Amazon region: Current and future variability and trends. *Front. Earth Sci.* **2018**, *6*, 228. [CrossRef]
- Artaxo, P. Amazon deforestation implications in local/regional climate change. *Proc. Natl. Acad. Sci. USA* **2023**, *120*, e2317456120. [CrossRef]
- Marengo, J.A.; Espinoza, J.C.; Fu, R.; Muñoz, J.C.J.; Alves, L.M.; DA Rocha, H.R.; Schöngart, J. Long-term variability, extremes and changes in temperature and hydrometeorology in the Amazon region: A review. *Acta Amaz.* **2024**, *54*, e54es22098. [CrossRef]
- Dutra, V.A.B.; Tavares, P.A.; de Lima, A.M.M.; Ribeiro, H.M.C. Anthropogenic environmental pressures in urban conservation units: A case study in Belém, Brazilian eastern Amazon. *Int. J. Hydro.* **2022**, *6*, 131–139. [CrossRef]
- Science Panel for the Amazon. *Amazon Assessment Report 2021*; Nobre, C., Encalada, A., Anderson, E., Roca Alcazar, F.H., Bustamante, M., Mena, C., Peña-Claros, M., Poveda, G., Rodrigues, J.P., Saleska, E., et al., Eds.; United Nations Sustainable Development Solutions Network: New York, NY, USA, 2021. Available online: <https://www.theamazonwewant.org/spa-reports> (accessed on 29 April 2024).
- de Souza, D.O.; Alvalá, R.C.S. Observational evidence of the urban heat island of Manaus City. *Brazil. Met. Apps* **2014**, *21*, 186–193. [CrossRef]
- Correa, P.B.; Candido, L.A.; Souza, R.A.F.; De Souza, R.A.F.; Andreoli, R.V.; Kayano, M.T. Estudo do fenômeno da ilha de calor na cidade de Manaus/AM: Um estudo a partir de dados de sensoriamento remoto, modelagem e estações meteorológicas. *Rev. Bras. Meteorol.* **2016**, *31*, 167–176. [CrossRef]
- Dias, T.S.S.; Souza, E.B.; Franco, V.S.; Pinto, Á.J.d.A.; Thales, M.C.; Mendoza, R.R.; Amaral, C.T.; Gonçalves, J.B.; Lima, I.F.; Pfeiff, G.K.; et al. Urban Environment and the Air Temperature Trend: The Case of the Metropolis of Brazilian Amazon. *Rev. Bras. De Geogr. Física* **2021**, *14*, 159–171. [CrossRef]
- Furtado, L.S.; Pereira, R.V.S.; de Souza, E.B. Hemeroby Mapping of the Belém Landscape in Eastern Amazon and Impact Study of Urbanization on the Local Climate. *Urban Sci.* **2024**, *8*, 15. [CrossRef]
- dos Santos, M.J.; Silva Dias, M.A.F.; Freitas, E.D. Influence of local circulations on wind, moisture, and precipitation close to Manaus City, Amazon Region, Brazil. *J. Geophys. Res. Atmos.* **2014**, *119*, 13233–13249. [CrossRef]
- Instituto Brasileiro de Geografia e Estatística (IBGE). Estimativas de População Publicadas no DOU—2024. Available online: <https://www.ibge.gov.br/estatisticas/sociais/populacao/9103-estimativas-de-populacao.html> (accessed on 2 July 2025).
- Paca, V.H.M.; Espinoza-Dávalos, G.E.; Moreira, D.M.; Comair, G. Variability of trends in precipitation across the Amazon river basin determined from the CHIRPS precipitation product and from station records. *Water* **2020**, *12*, 1244. [CrossRef]
- Funk, C.; Peterson, P.; Landsfeld, M.; Pedreros, D.; Verdin, J.; Shukla, S.; Husak, G.; Rowland, J.; Harrison, L.; Hoell, A.; et al. The climate hazards infrared precipitation with stations—A new environmental record for monitoring extremes. *Sci. Data* **2015**, *2*, 150066. [CrossRef] [PubMed]
- Funatsu, B.M.; Le Roux, R.; Arvor, D.; Espinoza, J.C.; Claud, C.; Ronchail, J.; Michot, V.; Dubreuil, V. Assessing precipitation extremes (1981–2018) and deep convective activity (2002–2018) in the Amazon region with CHIRPS and AMSU data. *Clim. Dyn.* **2021**, *57*, 827–849. [CrossRef]
- Souza, C.M., Jr.; Shimbo, J.Z.; Rosa, M.R.; Parente, L.L.; Alencar, A.; Rudorff, B.F.; Hasenack, H.; Matsumoto, M.; Ferreira, L.G.; Souza-Filho, P.W.M.; et al. Reconstructing Three Decades of Land Use and Land Cover Changes in Brazilian Biomes with Landsat Archive and Earth Engine. *Remote Sens.* **2020**, *12*, 2735. [CrossRef]
- World Meteorological Organization (WMO). Guidelines on the Calculation of Climate Normals. WMO-No. 1203. 2017. Available online: <https://library.wmo.int/idurl/4/55797> (accessed on 23 March 2023).
- Werth, D.; Avissar, R. The local and global effects of Amazon deforestation. *J. Geophys. Res. Atmos.* **2002**, *107*, LBA-55. [CrossRef]
- Jolliffe, I.T.; Cadima, J. Principal component analysis: A review and recent developments. *Phil. Trans. R. Soc. A* **2016**, *374*, 20150202. [CrossRef]
- Nobre, C.A.; Sampaio, G.; Borma, L.S.; Castilla-Rubio, J.C.; Silva, J.S.; Cardoso, M. Land-use and climate change risks in the Amazon and the need of a novel sustainable development paradigm. *Proc. Natl. Acad. Sci. USA* **2016**, *113*, 10759–10768. [CrossRef]
- Hirsch, R.M.; Slack, J.R.; Smith, R.A. Techniques of trend analysis for monthly water quality data. *Water Resour. Res.* **1982**, *18*, 107–121. [CrossRef]
- Sen, P.K. Estimates of the regression coefficient based on Kendall's tau. *J. Am. Stat. Assoc.* **1968**, *63*, 1379–1389. [CrossRef]

24. Trenberth, K.E.; Jones, P.D.; Ambenje, P.; Bojariu, R.; Easterling, D.; Tank, A.K.; Parker, D.; Rahimzadeh, F.; Renwick, J.A.; Rusticucci, M.; et al. Observations: Surface and Atmospheric Climate Change. In *Climate Change 2007: The Physical Science Basis. Contribution of Working Group I to the Fourth Assessment Report of the Intergovernmental Panel on Climate Change*; Solomon, S., Qin, D., Manning, M., Chen, Z., Marquis, M., Averyt, K.B., Tignor, M., Miller, H.L., Eds.; Cambridge University Press: Cambridge, UK; New York, NY, USA, 2007. Available online: <https://www.ipcc.ch/site/assets/uploads/2018/02/ar4-wg1-chapter3-1.pdf> (accessed on 10 December 2009).
25. Zhang, X.; Alexander, L.; Hegerl, G.C.; Jones, P.; Tank, A.K.; Peterson, T.C.; Trewin, B.; Zwiers, F.W. Indices for monitoring changes in extremes based on daily temperature and precipitation data. *WIREs Clim. Change* **2011**, *2*, 851–870. [[CrossRef](#)]
26. Alexander, L.V.; Zhang, X.; Peterson, T.C.; Caesar, J.; Gleason, B.; Tank, A.M.G.K.; Haylock, M.; Collins, D.; Trewin, B.; Rahimzadeh, F.; et al. Global observed changes in daily climate extremes of temperature and precipitation. *J. Geophys. Res.* **2006**, *111*, D05109. [[CrossRef](#)]
27. de Souza, E.B.; Ferreira, D.B.S.; Guimarães, J.T.F.; Franco, V.D.S.; de Azevedo, F.T.M.; de Moraes, B.C.; de Oliveira Ponte de Souza, P.J. Padrões climatológicos e tendências da precipitação nos regimes chuvoso e seco da Amazônia oriental. *Rev. Bras. Climatol.* **2017**, *21*, 81–93. [[CrossRef](#)]
28. Almeida, C.T.; Oliveira-Júnior, J.F.; Delgado, R.C.; Cubo, P.; Ramos, M.C. Spatiotemporal rainfall and temperature trends throughout the Brazilian Legal Amazon, 1973–2013. *Int. J. Climatol.* **2017**, *37*, 2013–2026. [[CrossRef](#)]
29. Terassi, P.M.B.; Galvani, E.; Gobo, J.P.A.; Oscar-Júnior, A.C.d.S.; Luiz-Silva, W.; Sobral, B.S.; de Gois, G.; Biffi, V.H.R. Exploring climate extremes in Brazil's Legal Amazon. *Stoch. Environ. Res. Risk Assess.* **2024**, *38*, 1403–1422. [[CrossRef](#)]
30. Da Silva, P.E.; Santos e Silva, C.M.; Spyrides, M.H.C.; Andrade, L.M.B. Precipitation and air temperature extremes in the Amazon and northeast Brazil. *Int. J. Climatol.* **2019**, *39*, 579–595. [[CrossRef](#)]
31. IPCC. Summary for Policymakers. In *Climate Change 2023: Synthesis Report. Contribution of Working Groups I, II and III to the Sixth Assessment Report of the Intergovernmental Panel on Climate Change*; Core Writing Team, Lee, H., Romero, J., Eds.; IPCC: Geneva, Switzerland, 2023; pp. 1–34. [[CrossRef](#)]
32. Cavalcante, R.B.L.; Ferreira, D.B.S.; Pontes, P.R.M.; Tedeschi, R.G.; da Costa, C.P.W.; de Souza, E.B. Evaluation of extreme rainfall indices from CHIRPS precipitation estimates over the Brazilian Amazonia. *Atmos. Res.* **2020**, *238*, 104879. [[CrossRef](#)]
33. Butt, E.W.; Baker, J.C.A.; Bezerra, F.G.S.; von Randow, C.; Aguiar, A.P.D.; Spracklen, D.V. Amazon deforestation causes strong regional warming. *Proc. Natl. Acad. Sci. USA* **2023**, *120*, e2309123120. [[CrossRef](#)] [[PubMed](#)]
34. De Lima, A.C.B.; Almeida, O.; Pinedo-Vasquez, M.; Lee, T.M.; Rivero, S.; Schramski, S.; Mansur, A.V. Climate hazards in small and medium cities in the Amazon Delta and Estuary: Challenges for resilience. *Environ. Urban.* **2019**, *32*, 195–212. [[CrossRef](#)]
35. Spracklen, D.V.; Baker, J.C.A.; Garcia-Carreras, L.; Marsham, J.H. The Effects of Tropical Vegetation On Rainfall. *Annu. Rev. Environ. Resour.* **2018**, *43*, 193–218. [[CrossRef](#)]
36. Caccamo, M.T.; Castorina, G.; Colombo, F.; Insinga, V.; Maiorana, E.; Magazù, S. Weather forecast performances for complex orographic areas: Impact of different grid resolutions and of geographic data on heavy rainfall event simulations in Sicily. *Atmos. Res.* **2017**, *198*, 22–33. [[CrossRef](#)]
37. Castorina, G.; Caccamo, M.T.; Colombo, F.; Magazù, S. The Role of Physical Parameterizations on the Numerical Weather Prediction: Impact of Different Cumulus Schemes on Weather Forecasting on Complex Orographic Areas. *Atmosphere* **2021**, *12*, 616. [[CrossRef](#)]
38. de Oliveira, J.V.; Cohen, J.; Barlage, M.; Silva Dias, M.A. The Influence of Urbanization on the Development of a Convective Storm—A Study for the Belém Metropolitan Region, Brazil. *Atmosphere* **2022**, *13*, 1026. [[CrossRef](#)]
39. Lovejoy, T.E.; Nobre, C. Amazon Tipping Point. *Sci. Adv.* **2018**, *4*, eaat2340. [[CrossRef](#)]

Disclaimer/Publisher's Note: The statements, opinions and data contained in all publications are solely those of the individual author(s) and contributor(s) and not of MDPI and/or the editor(s). MDPI and/or the editor(s) disclaim responsibility for any injury to people or property resulting from any ideas, methods, instructions or products referred to in the content.